NASA
Technical
Paper
2545

February 1986

Orifice-Induced Pressure Error Studies in Langley 7- by 10-Foot High-Speed Tunnel

E. B. Plentovich
and Blair B. Gloss

NASA

NASA
Technical
Paper
2545

1986

Orifice-Induced Pressure Error Studies in Langley 7- by 10-Foot High-Speed Tunnel

E. B. Plentovich
and Blair B. Gloss

Langley Research Center
Hampton, Virginia

National Aeronautics
and Space Administration

**Scientific and Technical
Information Branch**

SUMMARY

For some time it has been known that the presence of a static-pressure measuring hole will disturb the local flow field in such a way that the sensed static pressure will be in error. The results of previous studies aimed at studying the error induced by the pressure orifice were for relatively low Reynolds number flows. Because of the advent of high Reynolds number transonic wind tunnels, a study was undertaken to assess the magnitude of this error at higher Reynolds numbers than previously published and to study a possible method of eliminating this pressure error. This study was conducted in the Langley 7- by 10-Foot High-Speed Tunnel on a flat plate. The model was tested at Mach numbers from 0.40 to 0.72 and at Reynolds numbers from 7.7×10^6 to 11×10^6 per meter (2.3×10^6 to 3.4×10^6 per foot), respectively. The results indicated that as orifice size increased, the pressure error also increased but that a porous metal (sintered metal) plug inserted in an orifice could greatly reduce the pressure error induced by the orifice.

INTRODUCTION

For some time, it has been known that the presence of a static-pressure measuring hole drilled in and normal to a surface will disturb the local flow field such that the sensed static pressure will be in error (refs. 1 through 8). Ideally, the measuring hole should be infinitesimally small so as not to disturb the adjacent flow field; thereby, the orifice-induced pressure error will be eliminated. Reference 2 points out that, in subsonic flow, the basic pressure error caused by finite-sized orifices arises from a combination of three factors: (1) the streamlines diverging into the hole, (2) an eddy or system of eddies being generated in the hole, and (3) a pitot effect occurring at the downstream edge of the hole. These phenomena generally combine to produce a measured pressure which is too high; however, according to reference 3, pressures that are too low can occur when the hole depth is less than twice the hole diameter. The magnitude of this error is influenced by the following geometric factors: ratio of hole diameter to hole depth; inclination of the hole axis relative to the surface; and the condition of the hole entry with respect to roundness, burrs, and chamfer. Some aerodynamic factors, mentioned in reference 4, which influence the orifice-induced pressure error are the type of boundary layer present; the boundary-layer thickness; the local dynamic pressure and Mach number; and the pressure gradient present outside the boundary layer.

The results of the previous studies have mostly been limited to subsonic flow conditions where the hole diameter is no larger than four times the boundary-layer displacement thickness (refs. 1 through 6). However, for flow fields encountered in high Reynolds number wind tunnels, such as the National Transonic Facility (NTF) at the Langley Research Center (ref. 9), the boundary layers can be an order of magnitude thinner than that for conventional tunnels, and typical hole diameters may be 100 times the boundary-layer displacement thickness. Thus, the orifice-induced pressure error may become significantly larger than the errors previously reported for conventional wind tunnels (refs. 1 through 5).

Rainbird, reference 4, hypothesized that pressure error would increase with increasing ratios of orifice diameter to boundary-layer displacement thickness d/δ^*. However, the experiment by Franklin and Wallace (ref. 5) not only failed to confirm

this finding, but their data indicated a consistent correlation between $\Delta C_p/C_f$ and $R_d\sqrt{C_f/2}$ for all values of d/δ^* tested (where ΔC_p is static-pressure error, C_f is local skin friction coefficient, and R_d is Reynolds number based on hole diameter). These data also indicated that the induced pressure error would at most be a weak function of $R_d\sqrt{C_f/2}$ for values of $R_d\sqrt{C_f/2}$ greater than 1500. The present study extends the range of data previously reported to determine to what extent pressure error needs to be considered at high Reynolds numbers. Orifice-induced pressure error was studied for flow conditions where the range of both Reynolds number based on orifice diameter and the ratios of d/δ^* were larger than previously reported in references 1 through 8. Also described is a technique for reducing the orifice-induced pressure error by inserting a porous metal disk in the orifice. Some of these data have previously been reported in reference 10.

SYMBOLS

b	model span, cm
c	model chord, cm
C_f	local skin friction coefficient
C_p	coefficient of pressure
C_p^*	coefficient of pressure corresponding to sonic speed
d	static-pressure orifice diameter, cm
M	Mach number
p	measured static pressure, atm
$p_{"correct"}$	static pressure measured by porous plug orifice, atm
R	Reynolds number
t	time, sec
u	local velocity, cm/sec
V	free-stream velocity, cm/sec
X	chordwise distance measured from leading edge of model, cm
y	perpendicular distance measured from model surface through boundary layer, cm
Y	spanwise distance measured from flat-plate model centerline, cm
δ	boundary-layer thickness, cm
δ^*	boundary-layer displacement thickness, cm
ΔC_p	static-pressure error, $\dfrac{p_{measured} - p_{"correct"}}{1/2(\rho V^2)}$

η $= \frac{y}{b/2}$

ρ fluid density, kg/m^3

Subscripts:

d hole diameter

e edge of boundary layer

∞ free-stream conditions

Abbreviations:

B.L. boundary layer

ID inner diameter

MODEL DESCRIPTION

The flat-plate model is sketched in figures 1 and 2. It was supported on four long legs to help reduce blockage from equipment below the plate. Guy wires were attached to either side of the plate to help increase lateral stiffness and stability. Ninety-one 0.051-cm-diameter (0.020-in.) orifices were arranged over the upper surface of the plate, as shown in figure 2, in order to resolve pressure gradients on the plate. Also note the leading-edge contour and the adjustable trailing-edge flap which were designed to keep the stagnation point at the leading edge and thereby create a zero-pressure-gradient flow over the upper surface of the plate. Five large holes located along the centerline of the plate (fig. 2) were used for installation of either the interchangeable test orifices or the boundary-layer rake, the two configurations in which the plate could be tested. Figure 3 is a photograph of the model installed in the Langley 7- by 10-Foot High-Speed Tunnel (7 × 10 HST) configured with the boundary-layer rake installed. The boundary-layer rake, sketched in figure 4, was used to measure total pressure through the boundary layer. The rake had a single probe which traversed the boundary layer and was powered by a motor which was located below the plate. (See fig. 3.)

Figure 5 is a photograph of the configuration with a test orifice installed in one of the centerline holes. A schematic drawing showing the construction of the interchangeable test orifices is provided as figure 6. Three sizes of interchangeable orifices were tested. The inner diameters were 0.330 cm (0.130 in.), 0.660 cm (0.260 in.), and 1.321 cm (0.520 in.) for orifices I, II, and III, respectively. Since only one size orifice was tested at one location on each run, 0.051-cm-diameter orifices were made to fit in the test orifice locations not in use during that run. After testing was completed on the configuration, the 1.321-cm-diameter orifice was modified, as shown in figure 6, to accept a circular disk of sintered metal (porous metal) which was press fitted into the orifice flush with the upper surface. Figure 7 shows a top view of a porous plug installed in an orifice. The plumbing used to connect the orifice to the pressure transducer was a piece of flexible tubing 3.175 cm (1.25 in.) in diameter and 30.48 m (100 ft) in length, which was located beneath the tunnel floor. Orifice II and the associated plumbing were scaled to represent a 0.025-cm-diameter (0.010-in.) orifice and a length of 121.9 cm (4 ft) tubing which had an inner diameter of 0.13 cm (0.050 in.) in the Langley 0.3-Meter Transonic Cryogenic Tunnel (0.3-m TCT) (refs. 11 and 12).

APPARATUS AND TEST

The present investigation was conducted in the NASA Langley 7 × 10 HST (ref. 13), which is a subsonic, continuous-flow, atmospheric tunnel capable of operating over the Mach number range of 0.08 to 0.94. The plate was carefully aligned in the tunnel in order to have zero pitch and yaw angles relative to the free stream.

The model was tested at Mach numbers from 0.40 to 0.72 corresponding to Reynolds numbers of about 7.7×10^6 to 11×10^6 per meter (2.3×10^6 to 3.4×10^6 per foot), respectively. All tests were made with the boundary-layer transition fixed on the model by means of a strip of No. 120 grit 2.54 mm (0.10 in.) wide placed 1.40 cm (0.55 in.) aft of the leading edge; dimensions were calulated by using the criteria in reference 14.

DISCUSSION OF RESULTS

The measured pressure distribution at $M = 0.40$ and 0.72 and at Reynolds numbers of 7.7×10^6 and 11×10^6 per meter (2.3×10^6 and 3.4×10^6 per foot) is shown in figure 8(a) and (b), respectively. These pressure distributions show a substantial pressure peak in the leading-edge region of the flat plate; in fact, figure 8(b) seems to indicate that near the plate leading edge, a shock wave is present on the upper surface with the rake drive installed on the lower surface. The flat plate had been chosen as the holder for the test orifices in order to obtain a zero or nearly zero-pressure-gradient flow so that the data could be compared with previous data. The trailing-edge flap had been added to the model and the leading edge was contoured in an attempt to reduce the pressure peaks at the leading edge, but as can be seen in figure 8, these were not effective in reducing the leading-edge pressure peaks.

The major factor contributing to the pressure peak, the pressure gradient, and the ineffectiveness of the trailing-edge flap was the substantial amount of blockage from the hardware on the underside of the plate. This hardware can be seen in figures 3 and 5. The hardware located on the underside of the plate has about the same percentage of blockage, roughly 10 percent of the area under the plate, for each configuration. The tunnel blockage, based on the model frontal area, was about 2 percent. Although there was a strong pressure gradient at the leading edge, in the region of the test orifices the longitudinal pressure gradient was nearly nonexistent or had a slightly adverse pressure recovery region, as can be seen in figure 9. Since nearly zero-pressure-gradient flow had been achieved over the test orifices and δ^* was also measured, it was felt that the present data could be fairly compared with previous flat-plate data. Near the test orifice locations some of the pressure measurements are seen to be slightly disturbed; this is due to the influence of the boundary-layer survey mechanism on the orifice. The data in figure 9 showing the influence of the rake motor and drive were obtained with the survey rake removed and the motor and drive mounted at the second test orifice location. (See fig. 4.) The data showing the influence of the test orifice and plumbing were obtained with the 0.051-cm test orifice mounted in the first test orifice location.

Boundary-Layer Measurements

The boundary-layer survey rake, illustrated in figure 4, was designed so that total-pressure surveys through the boundary layer could be obtained at the first four test orifice locations. (See fig. 2.) For these boundary-layer measurements, a reference orifice of 0.051 cm diameter was installed at each test orifice location on

the plate. This small orifice was used to obtain a static-pressure measurement for use in the boundary-layer calculations. The data in figure 10 show that the effect of the total-pressure rake on the static pressure in the vicinity of the test orifice is small when the rake is at the outer edge of the boundary layer. However, as the rake approaches the surface of the plate, the static pressure at the test location is strongly affected. The reference static pressure for all boundary-layer calculations was obtained when the rake was at the outer edge of the boundary layer.

Shown in figure 11 are typical Mach number distributions measured through the boundary layer. The Mach number distributions were used in the equation

$$\delta^* = \int_0^{\delta} \left(1 - \frac{\rho u}{\rho_e u_e}\right) dy = \int_0^{\delta} \left(1 - \frac{M}{M_e}\sqrt{\frac{1 + 0.2M^2}{1 + 0.2M_e^2}}\right) dy$$

obtained from reference 15, to calculate the boundary-layer displacement thickness, where M_e is the Mach number at the edge of the boundary layer. In using this equation to calculate δ^*, it was assumed that the total temperature and the static pressure through the boundary layer remained constant.

Time-Averaged Pressure Error

As figure 2 shows, at each test orifice location there is a spanwise row of 0.051-cm-diameter orifices. By plotting the spanwise pressure distribution, a reference pressure level may be obtained. Typical plots of static pressure as a function of spanwise location on the plate for each test orifice are shown in figure 12. These data were obtained by test orifices located at the first two test orifice locations on the plate and are representative of all data obtained at each test orifice location. The data obtained at the third test orifice location are not shown as the porous plug orifice was damaged after being tested in the first two test orifice locations. For the conditions tested, the data clearly show that orifice-induced pressure error is a function of the orifice diameter and that the porous metal plug eliminates the orifice error associated with the largest orifice, orifice III. The same results are shown in figure 13 for $M = 0.40$ at the first test location, where orifice pressure error is plotted as a function of orifice diameter. For the calculation of ΔC_p, $p_{\text{"correct"}}$ was taken to be the result obtained by the porous plug orifice; this was substantiated by figure 12, where it was seen that the average of the pressures measured by the 0.051-cm-diameter orifices in the two-dimensional region on the flat plate was nearly that measured by the porous plug orifice.

Orifice-induced pressure error data are usually presented in the form of $\Delta C_p/C_f$ as a function $R_d\sqrt{C_f/2}$ (refs. 2 and 4 through 6), as shown in figure 14. Data obtained by Franklin and Wallace (ref. 5) are compared with the present experimental results in this figure. The Franklin and Wallace data were obtained at subsonic conditions in zero-pressure-gradient flow. For theoretical flat-plate flow, flow with zero pressure gradient, there are several methods available for calculating local skin friction based on the experimentally determined total-pressure profile through the boundary layer (refs. 16 and 17). However, the definition of the profile close to the plate was not adequate for consistent skin friction estimation. To estimate C_f at each orifice location, the charts given in reference 18 were used. These

charts assume a zero-pressure-gradient flow over the model. Because a pressure peak did exist at the leading edge, which is not typical of flat-plate flow (fig. 8), some error will be introduced into the estimation of C_f obtained from the charts. Even though there is considerable data scatter, due primarily to the local skin friction estimation, the data seem to indicate an increasing orifice-induced pressure error in this Reynolds number range. (See fig. 14.)

To investigate the effect of d/δ^* on orifice-induced pressure error, a plot of pressure error as a function of d/δ^* is given in figure 15. These data indicate that the pressure error is a function of d/δ^*, at least for the range of d/δ^* and Reynolds number covered in the present study. It is seen that at a d/δ^* of 12, the pressure error is approximately twice that at a d/δ^* of 2.

Unsteady Pressure Error

Shown in figure 16 are typical time histories of the pressure measured at the closed end of the orifice and plumbing system. These traces show the fluctuations in the measured pressure which were recorded on a strip chart recorder, and as such, no quantitative analysis was performed. The traces for a given Mach number were compared with each other by assuming that at time equal to zero the 0.051-cm-diameter orifice had zero variation in pressure. The data in figures 12 and 13 indicated that the pressure reading obtained by using the 0.051-cm orifice was slightly greater in magnitude than that obtained by using the porous metal plug; this difference is also apparent in the data in figure 16. For both Mach numbers, 0.40 and 0.72, shown in figure 16, a frequency of approximately 9 Hz is evident for orifice III without the porous metal plug. It is interesting to note that the first overtone frequency for a pipe closed on one end, 30.48 m (100 ft) in length, is approximately 9 Hz also. Further, this same frequency, with reduced amplitude, is evident on the trace for orifice III with the porous metal plug. Note that orifice III, if scaled to the appropriate size for the 0.3-m TCT, would be 0.051 cm in diameter, which is larger than the size conventionally used. With orifices and plumbing sized for typical wind-tunnel models, viscous effects may damp the system sufficiently so that resonant effects will be of no concern. Viscous damping at the orifice is probably the cause of the lack of resonance for the smaller orifices shown in figure 16.

CONCLUDING REMARKS

With the advent of high Reynolds number wind tunnels, the boundary layers on the models being tested in these facilities have become much thinner. Since the boundary-layer thickness can be much smaller than the orifice diameter at high Reynolds numbers, it was necessary to extend the orifice-induced pressure error data base that was currently available.

To study the effects of higher Reynolds numbers on pressure error, a test was conducted on a flat-plate model in the Langley 7- by 10-Foot High-Speed Tunnel. Several orifices of different diameters, which were scaled and modeled based on the orifices used in the Langley 0.3-Meter Transonic Cryogenic Tunnel, were tested. Since the tests were made in a conventional atmospheric wind tunnel, the test orifices were several times the size of conventional orifices to enable the ratio of orifice diameter to boundary-layer displacement thickness to be increased. This effectively simulated conditions at increased values of Reynolds number. The range of the ratio of orifice diameter to boundary-layer displacement thickness was extended to 12, an increase of 3 times what had been available. The results of these

studies indicate that over the range of Reynolds number and ratio of orifice diameter to boundary-layer displacement thickness covered, the orifice-induced pressure error is a function of the ratio of orifice diameter to boundary-layer displacement thickness and, when a sintered metal disk is inserted into an orifice, the orifice-induced pressure error is virtually eliminated. The sintered metal disk would also eliminate errors associated with holes that are not round or have burrs or chamfering.

NASA Langley Research Center
Hampton, VA 23665-5225
November 15, 1985

REFERENCES

1. Rayle, R. E.: Influence of Orifice Geometry on Static Pressure Measurements. ASME Paper No. 59-A-234, Nov.-Dec. 1959.

2. Shaw, R.: The Influence of Hole Dimensions on Static Pressure Measurements. J. Fluid Mech., vol. 7, pt. 4, Apr. 1960, pp. 550-564.

3. Livesey, J. L.; Jackson, J. D.; and Southern, C. J.: The Static Hole Error Problem: An Experimental Investigation of Errors for Holes of Varying Diameters and Depths. Aircr. Eng., vol. 34, no. 396, Feb. 1962, pp. 43-47.

4. Rainbird, W. J.: Errors in Measurement of Mean Static Pressure of a Moving Fluid Due to Pressure Holes. Nat. Res. Counc. Can. Quart. Bull., no. 3, 1967, pp. 58-89.

5. Franklin, R. E.; and Wallace, James M.: Absolute Measurements of Static-Hole Error Using Flush Transducers. J. Fluid Mech., vol. 42, pt. 1, June 4, 1970, pp. 33-48.

6. Kuwano, H.; Wu, J. M.; and Moulden, T. H.: An Experimental Study of Orifice Size on Static Pressure Measurements. Proceedings of the Twelfth International Symposium on Space Technology and Science, Nagasu, ed., AGNE Publ., Inc., 1977, pp. 175-180.

7. Reed, T. D.; Pope, T. C.; and Cooksey, J. M.: Calibration of Transonic and Supersonic Wind Tunnels. NASA CR-2920, Nov. 1977.

8. Pugh, P. G.; Peto, J. W.; and Ward, L. C.: Experimental Verification of Predicted Static Hole Size Effects on a Model With Large Streamwise Pressure Gradients. C.P. No. 1139, British A.R.C., 1971.

9. Igoe, William B.: Characteristics and Status of the U.S. National Transonic Facility. Cryogenic Wind Tunnels, AGARD-LS-111, July 1980, pp. 17-1 - 17-11.

10. Plentovich, E. B.; and Gloss, B. B.: Effects of Reynolds Number on Orifice Induced Pressure Error. AIAA-82-0613, Mar. 1982.

11. Kilgore, Robert A.: Design Features and Operational Characteristics of the Langley 0.3-Meter Transonic Cryogenic Tunnel. NASA TN D-8304, 1976.

12. Ray, Edward J.; Ladson, Charles L.; Adcock, Jerry B.; Lawing, Pierce L.; and Hall, Robert M.: Review of Design and Operational Characteristics of the 0.3-Meter Transonic Cryogenic Tunnel. NASA TM-80123, 1979.

13. Fox, Charles H., Jr.; and Huffman, Jarrett K.: Calibration and Test Capabilities of the Langley 7- by 10-Foot High Speed Tunnel. NASA TM X-74027, 1977.

14. Braslow, Albert L.; Hicks, Raymond M.; and Harris, Roy V., Jr.: Use of Grit-Type Boundary-Layer-Transition Trips on Wind-Tunnel Models. NASA TN D-3597, 1966.

15. Peterson, John B., Jr.: Boundary-Layer Velocity Profiles Downstream of Three-Dimensional Transition Trips on a Flat Plate at Mach 3 and 4. NASA TN D-5523, 1969.

16. Allen, Jerry M.: Use of Baronti-Libby Transformation and Preston Tube Calibrations To Determine Skin Friction From Turbulent Velocity Profiles. NASA TN D-4853, 1968.

17. Allen, Jerry M.; and Tudor, Dorothy H.: Charts for Interpolation of Local Skin Friction From Experimental Turbulent Velocity Profiles. NASA SP-3048, 1969.

18. Clutter, Darwin W.: Charts for Determining Skin-Friction Coefficients on Smooth and on Rough Flat Plates at Mach Numbers up to 5.0 With and Without Heat Transfer. Rep. No. ES 29074, Douglas Aircraft Co., Inc., Apr. 15, 1959.

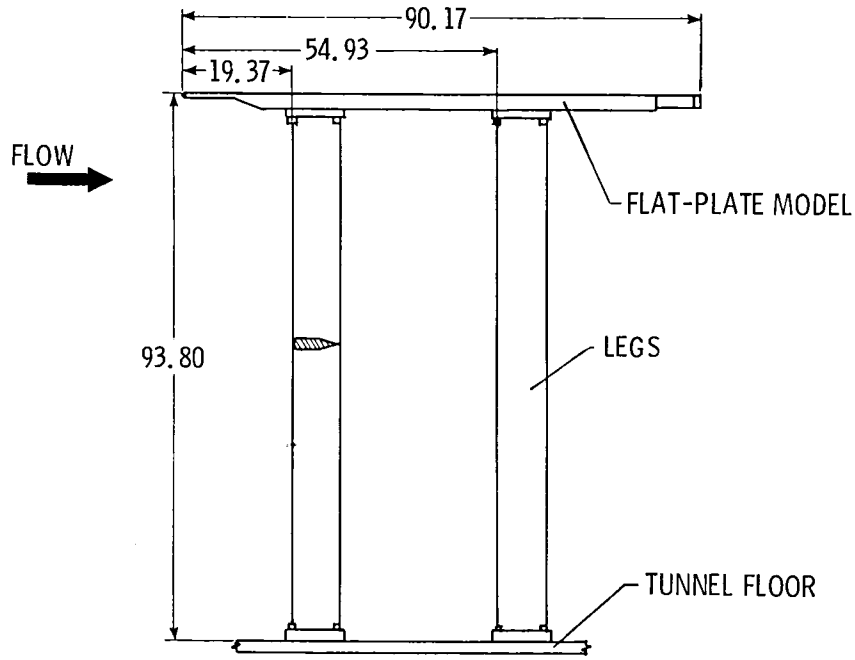

(a) Side view.

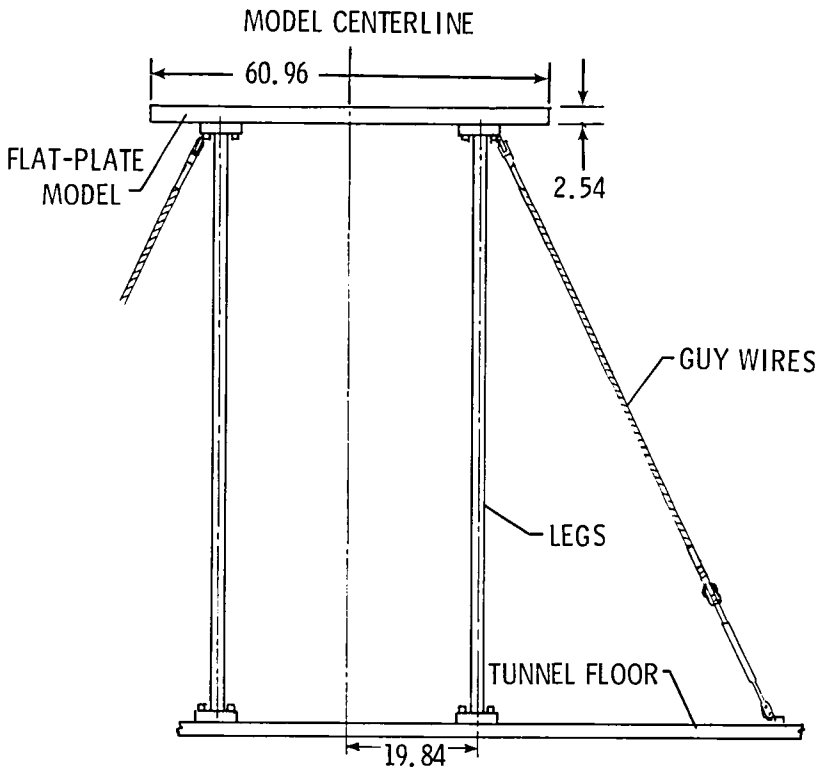

(b) Front view.

Figure 1.- Sketch of flat-plate model. All dimensions are in centimeters.

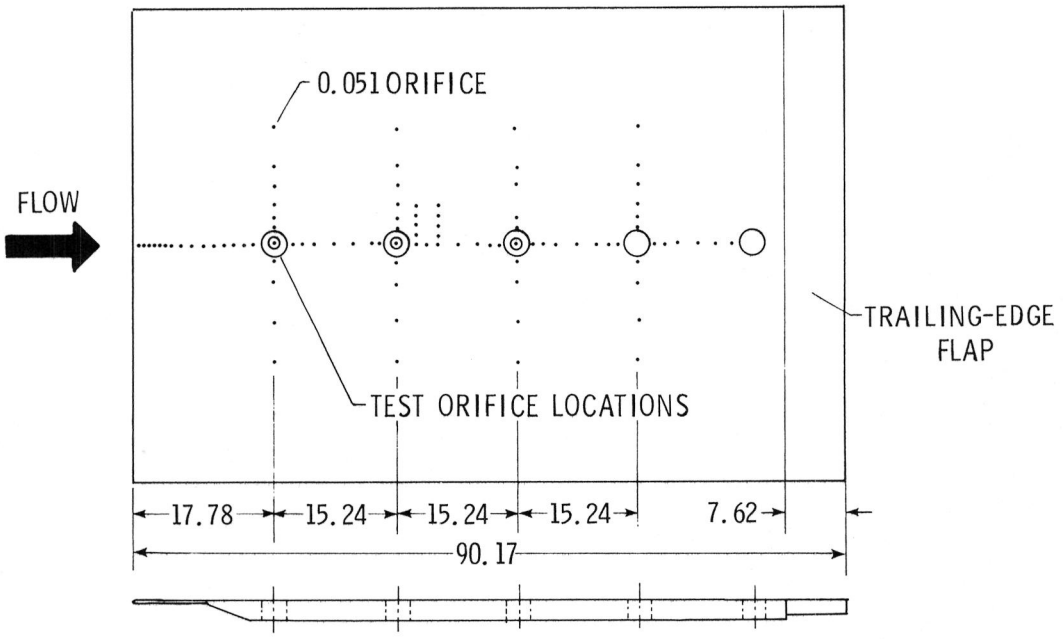

Figure 2.- Planform view of flat-plate model. All dimensions are in centimeters.

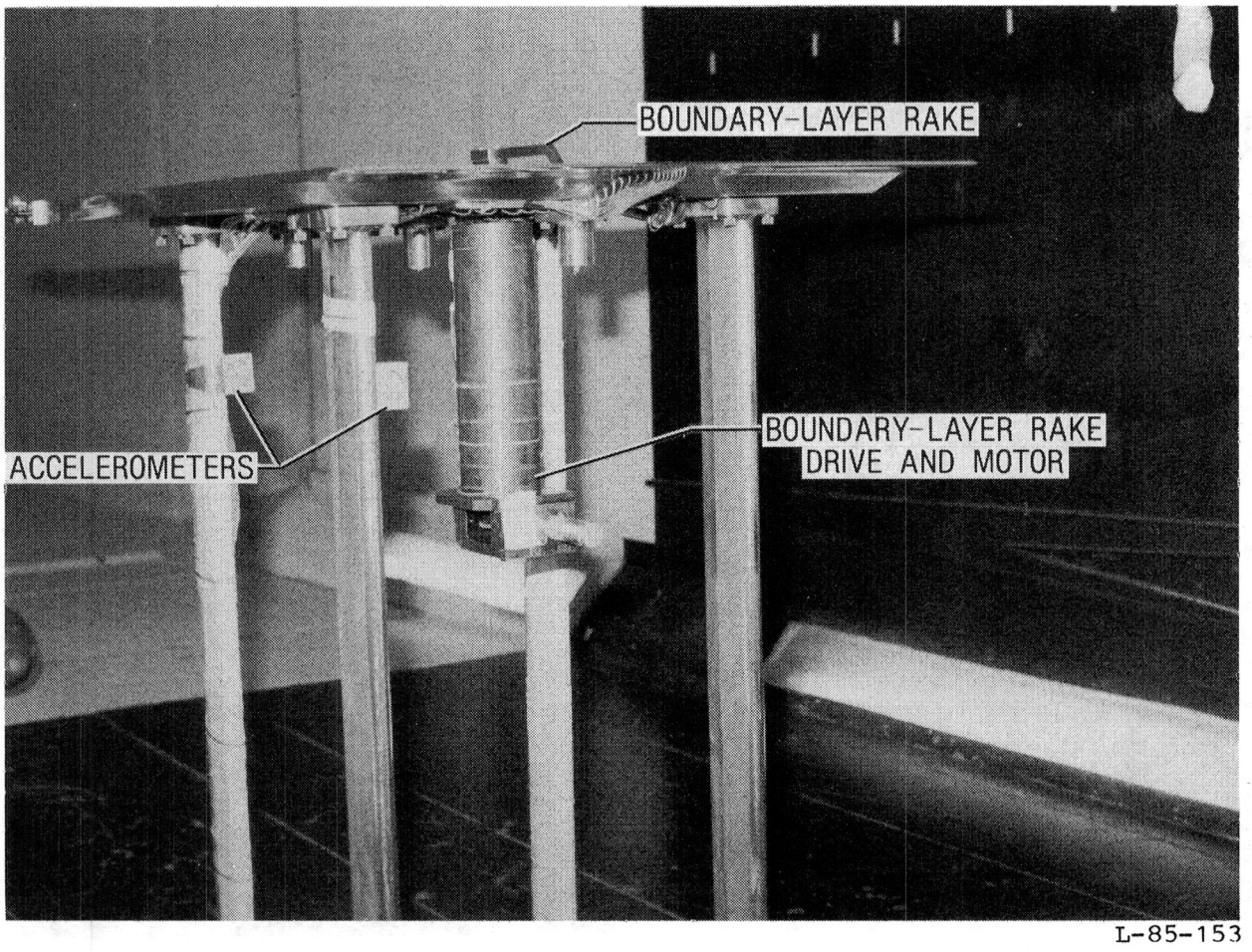

Figure 3.- Boundary-layer survey configuration.

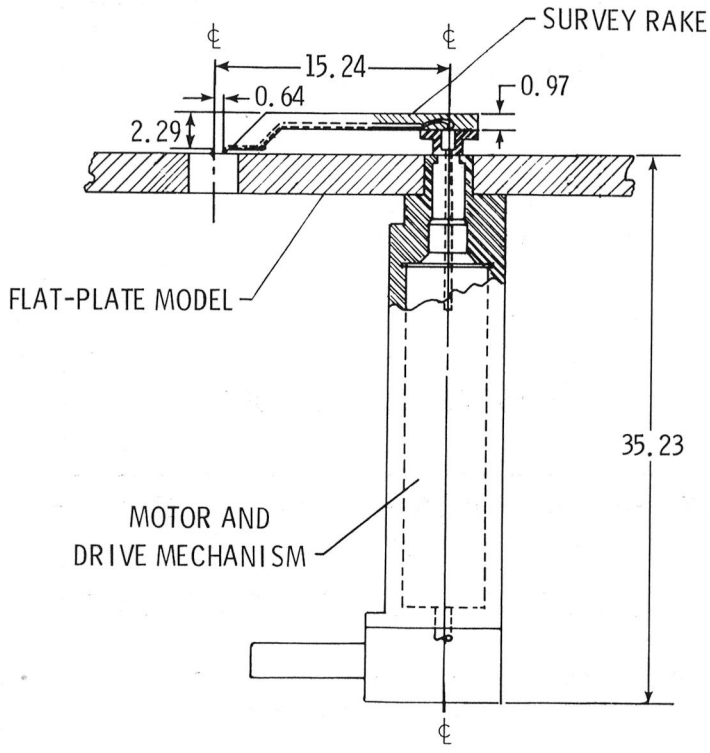

Figure 4.- Sketch of boundary-layer rake.
All dimensions are in centimeters.

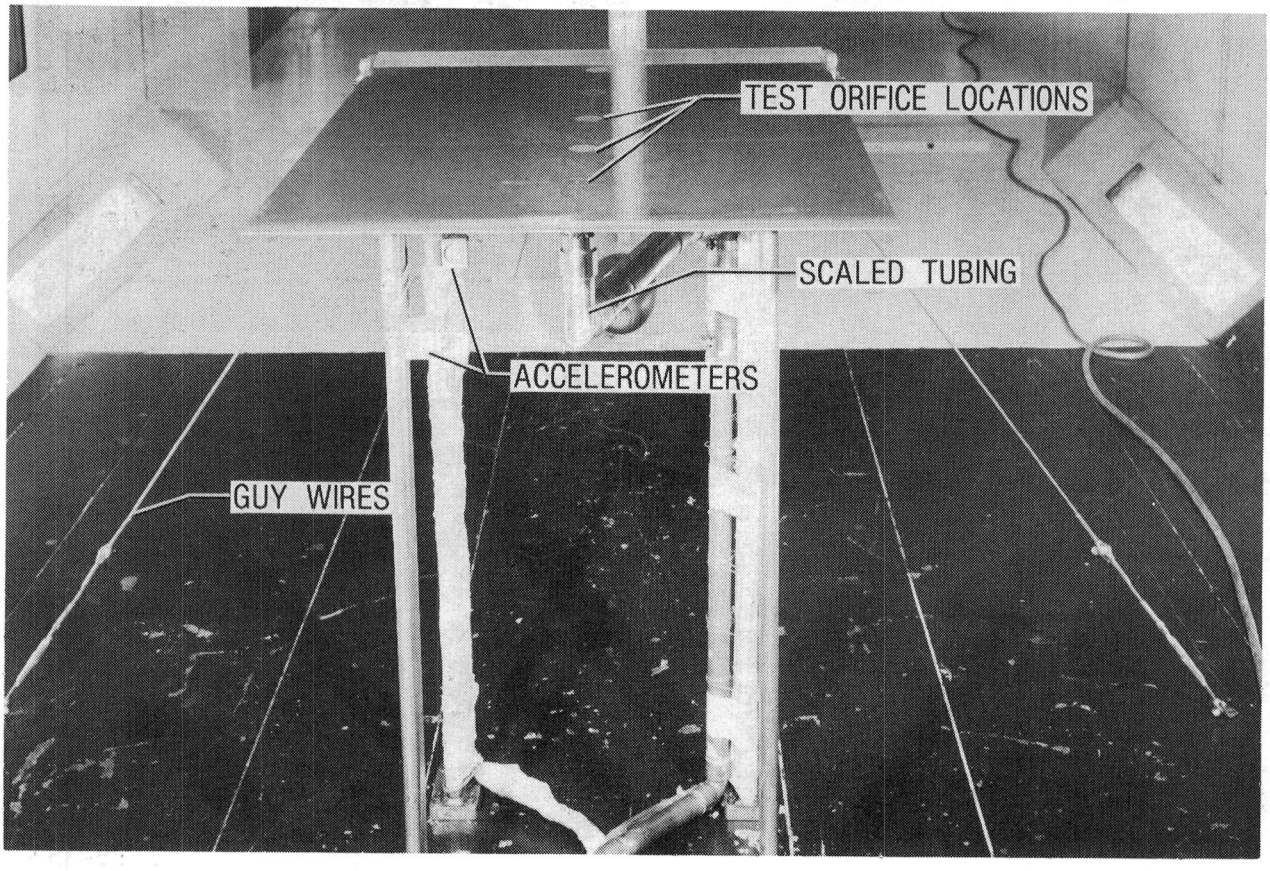

Figure 5.- Test orifice configuration.

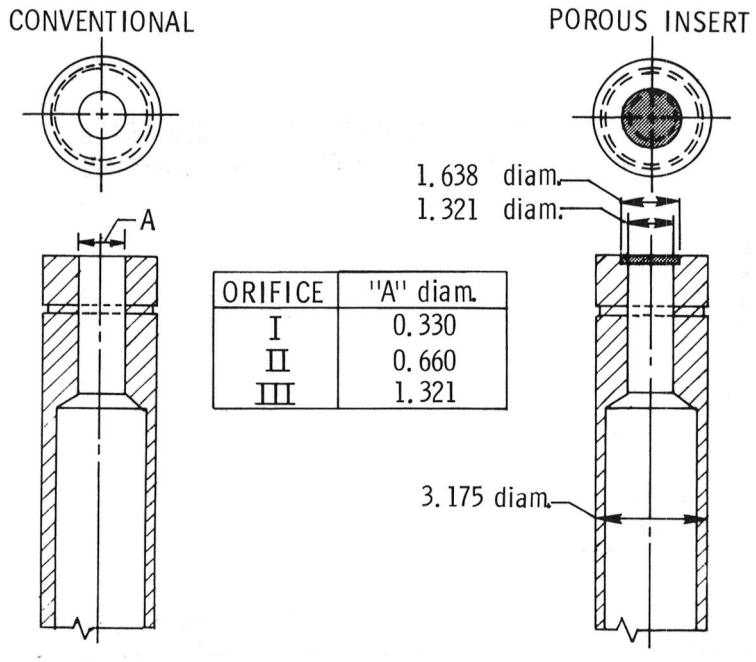

ORIFICE	"A" diam.
I	0.330
II	0.660
III	1.321

Figure 6.- Test orifice geometry. All dimensions are in centimeters.

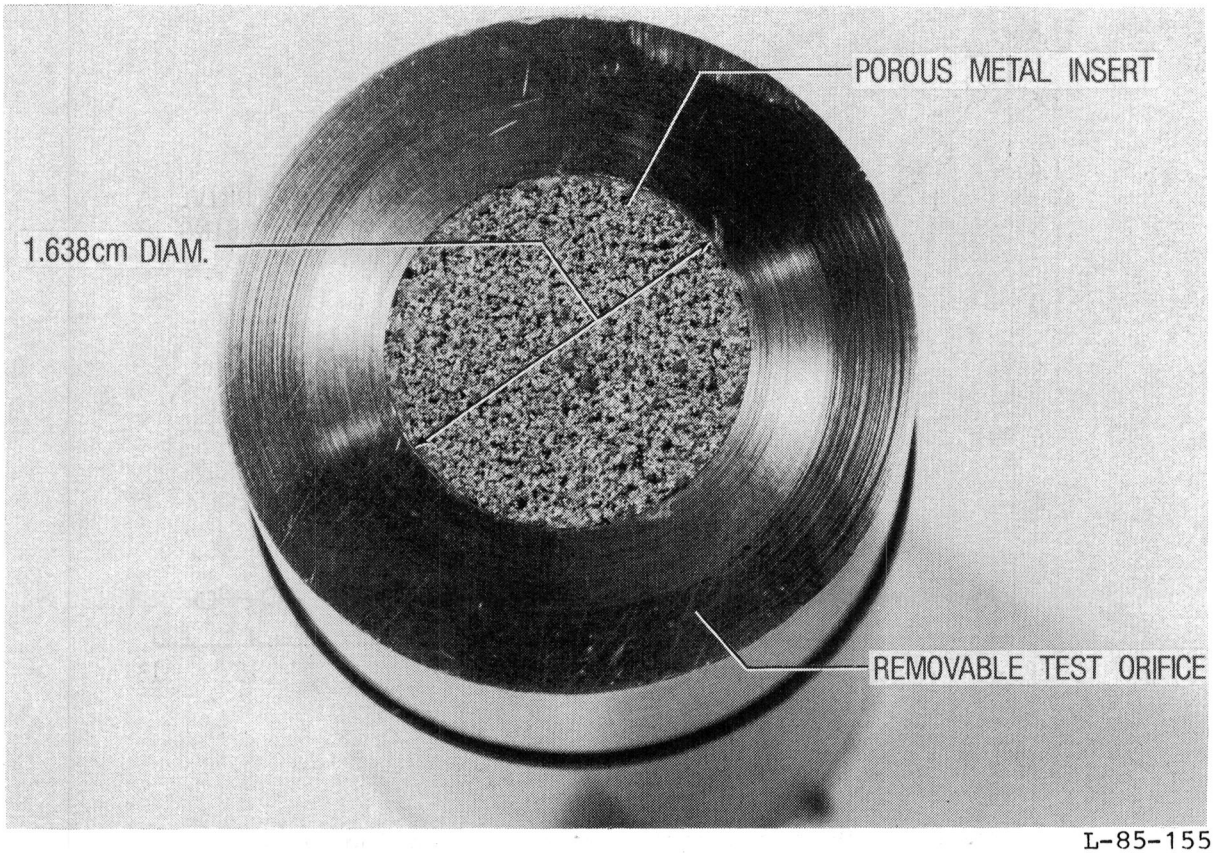

L-85-155

Figure 7.- Porous metal plug orifice.

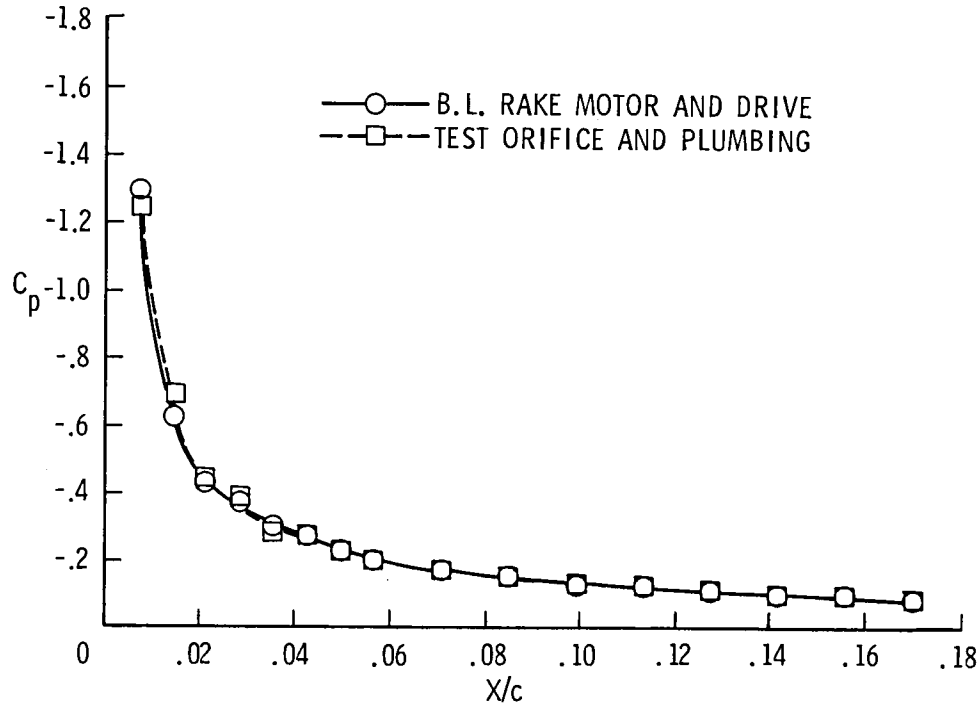

(a) Mach number = 0.40.

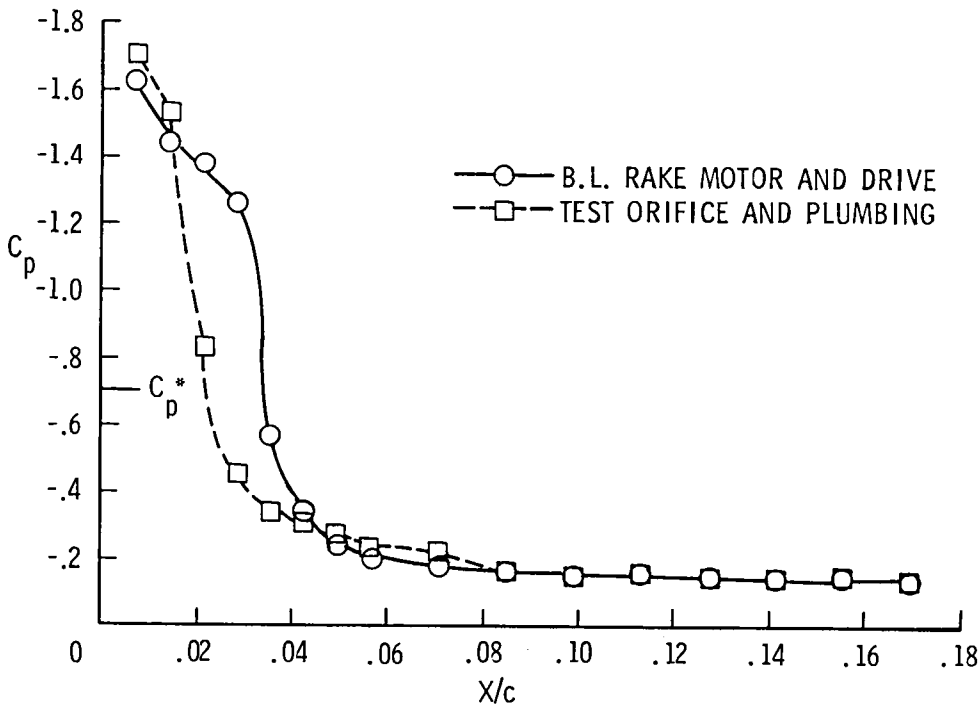

(b) Mach number = 0.72.

Figure 8.- Pressure distribution at leading edge of flat-plate model.

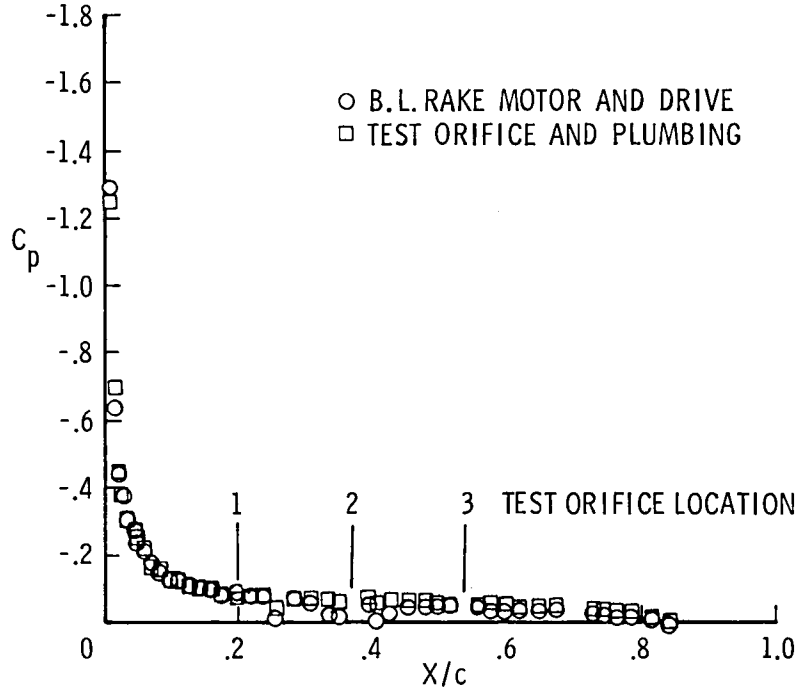

(a) Mach number = 0.40.

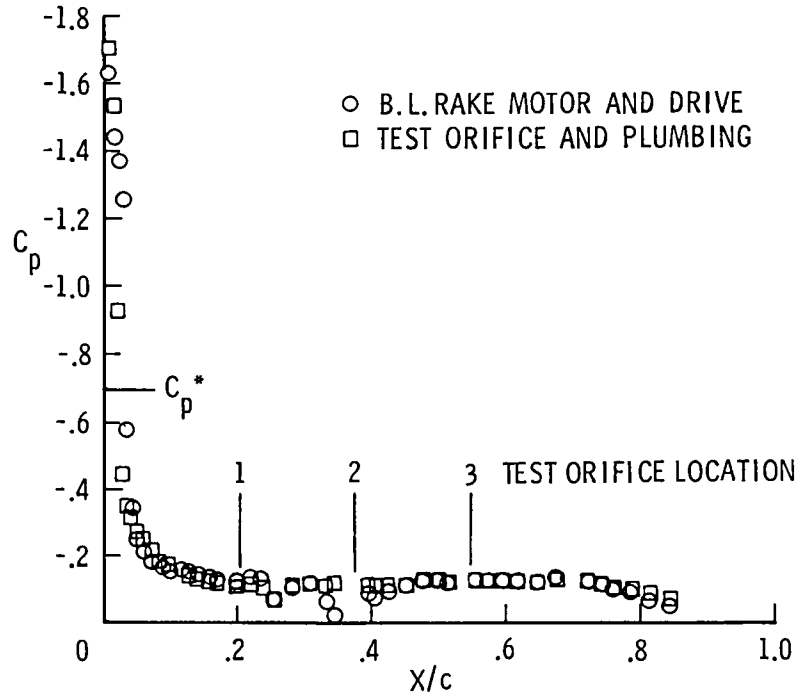

(b) Mach number = 0.72.

Figure 9.- Pressure distribution along centerline of flat-plate model.

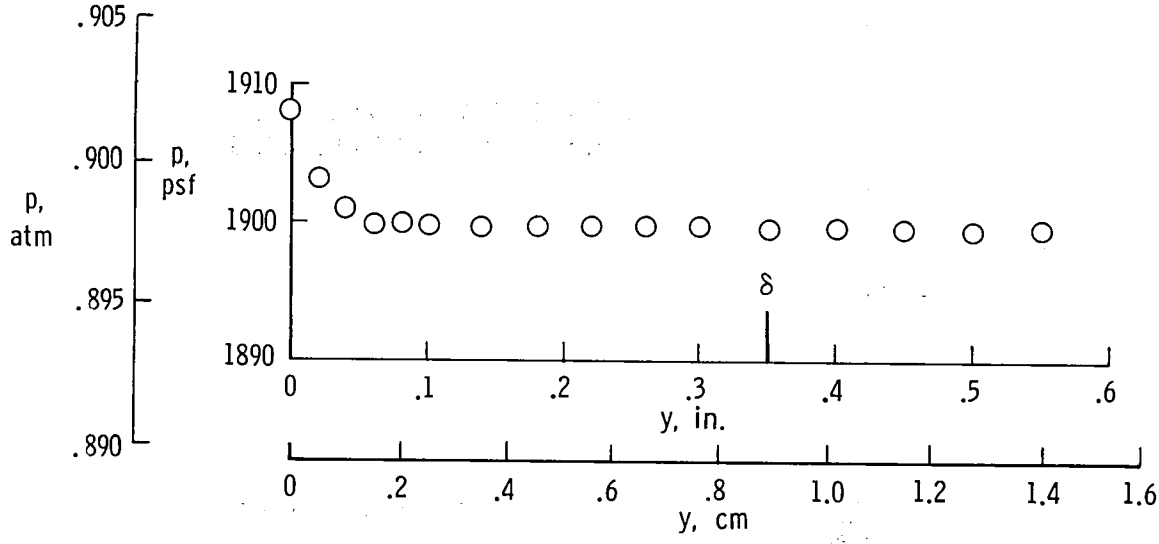

(a) Mach number = 0.40.

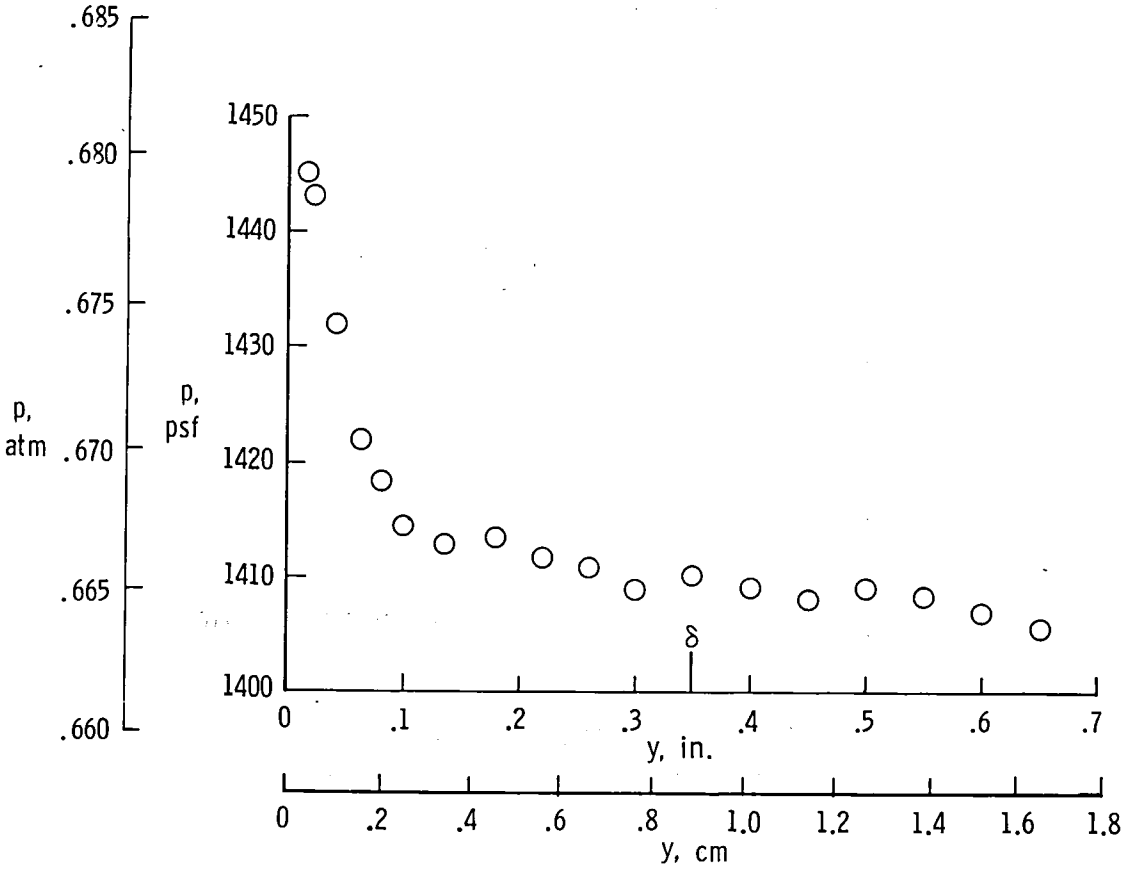

(b) Mach number = 0.72.

Figure 10.- Static pressure at model as function of boundary-layer rake position.

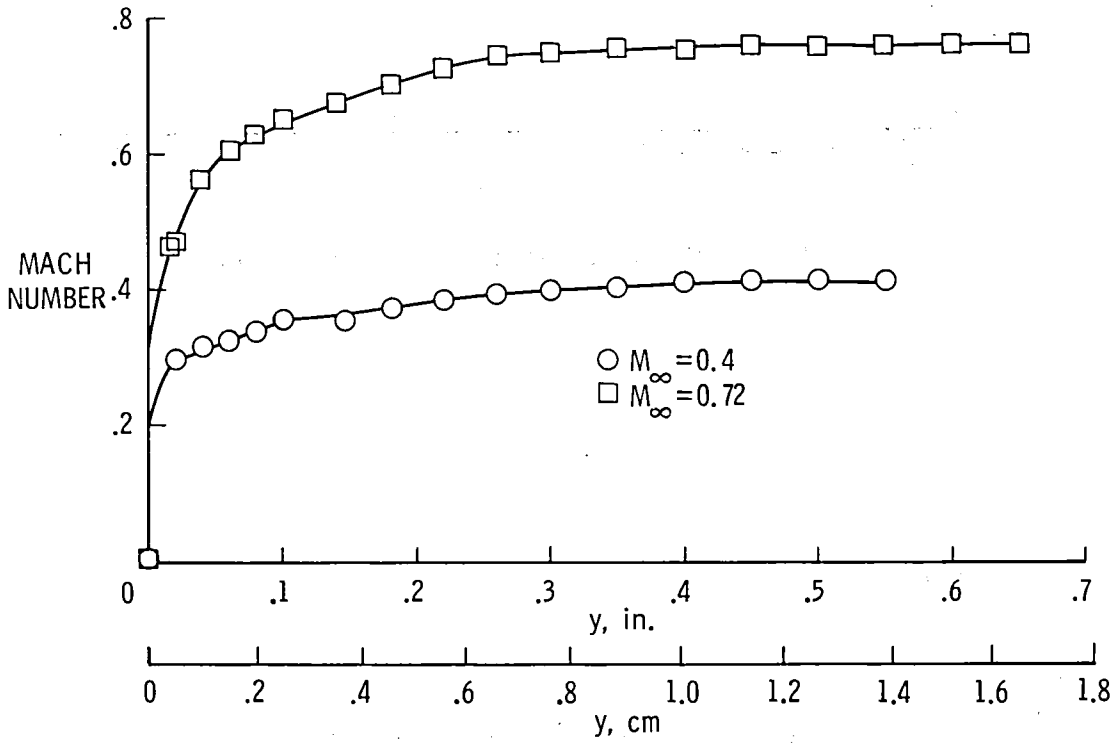

Figure 11.- Mach number distribution through boundary layer at test orifice location 2.

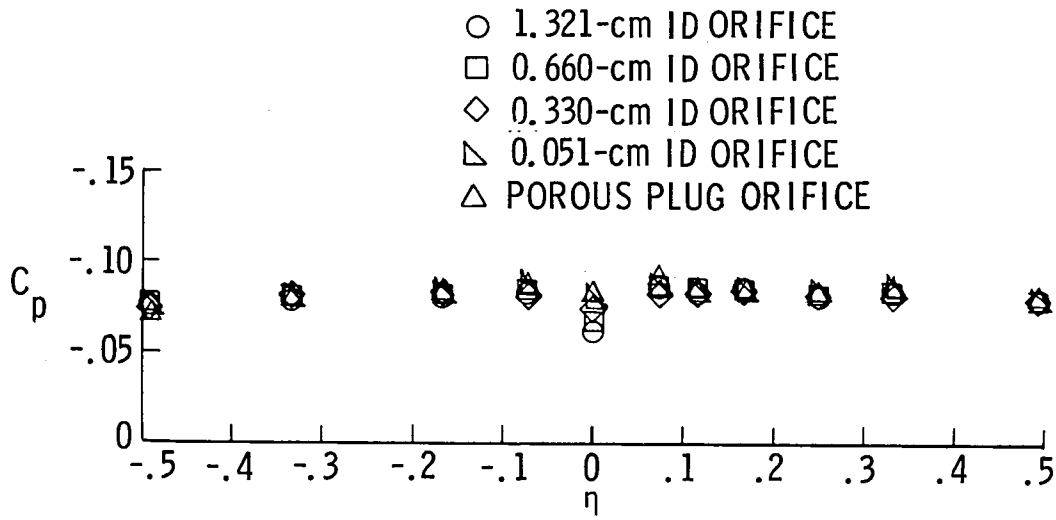

(a) Test orifice location 1 (X/c = 0.20).

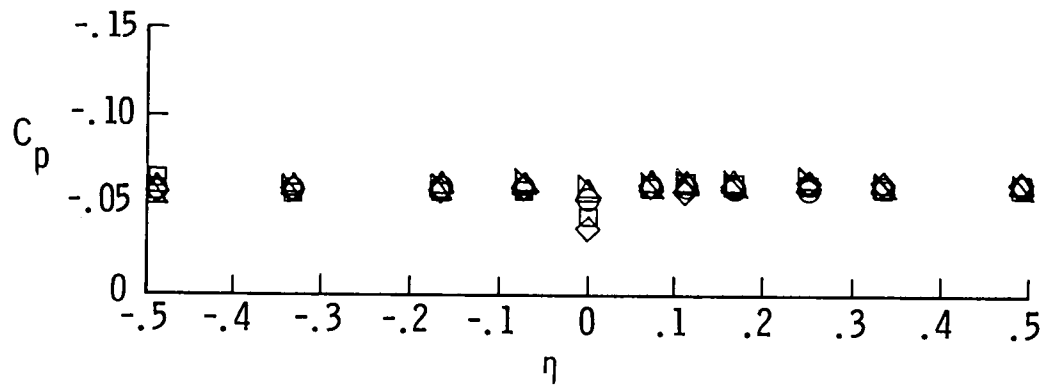

(b) Test orifice location 2 (X/c = 0.37).

Figure 12.- Spanwise pressure distribution on model showing effect of orifice size on pressure error at M = 0.40. Symbol denotes run where specified orifice was on model centerline.

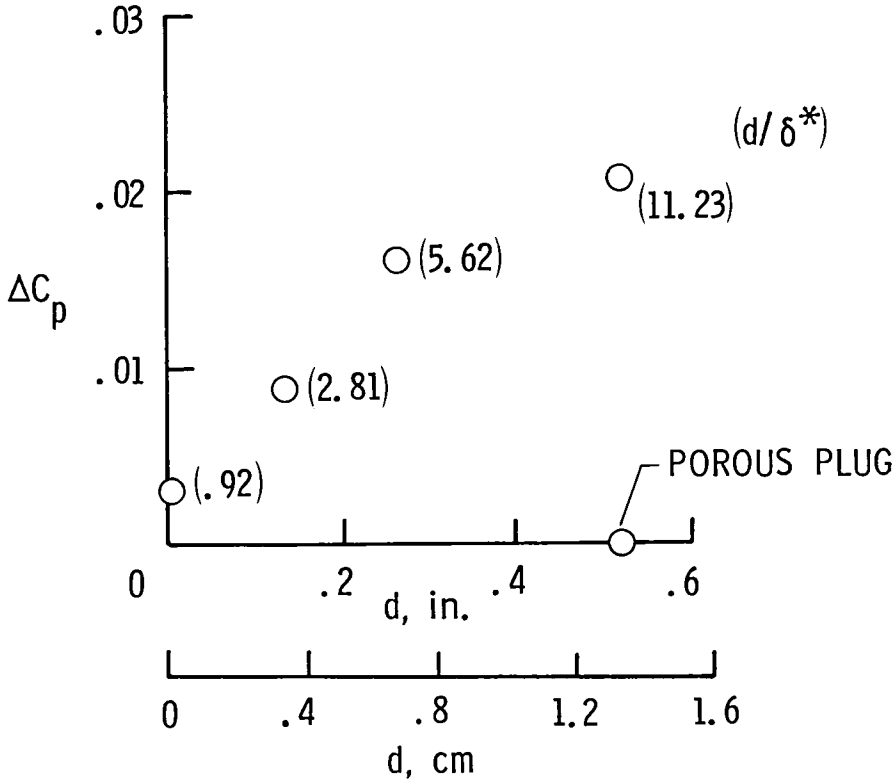

Figure 13.- Effect of orifice size on pressure error at M = 0.40, test orifice location 1.

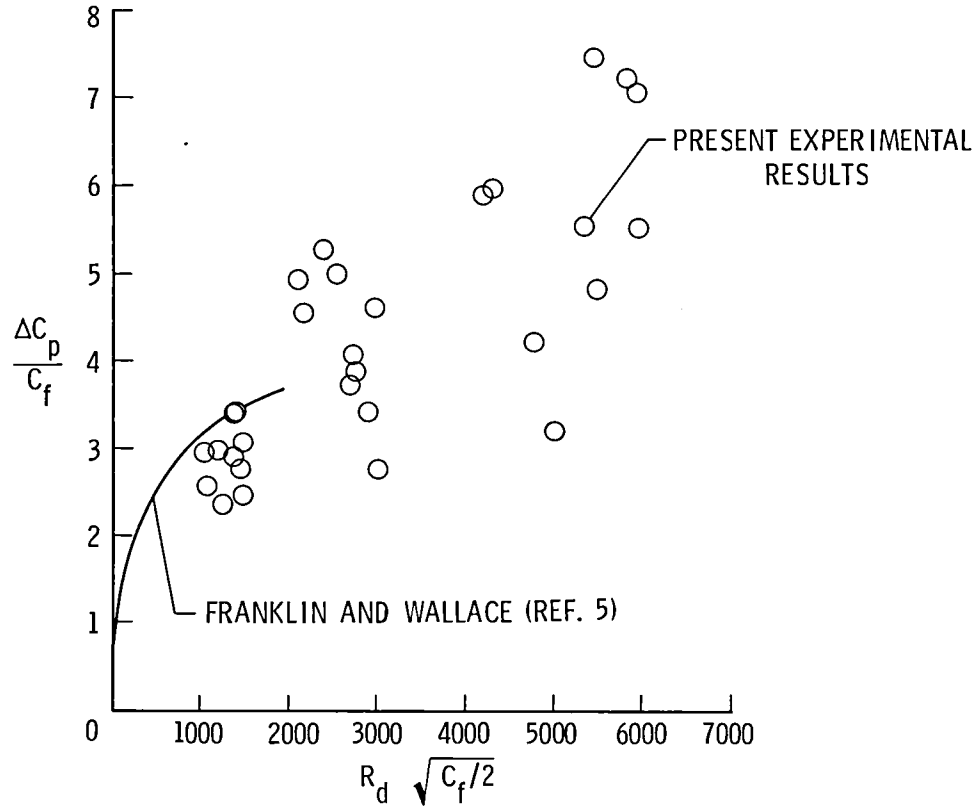

Figure 14.- Effect of Reynolds number on orifice-induced pressure error.

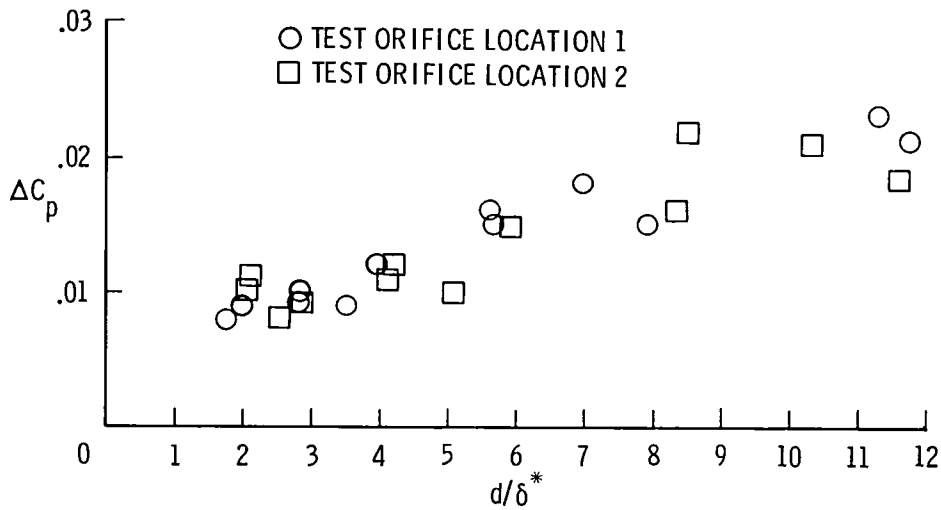

Figure 15.- Effect of d/δ^* on pressure error.

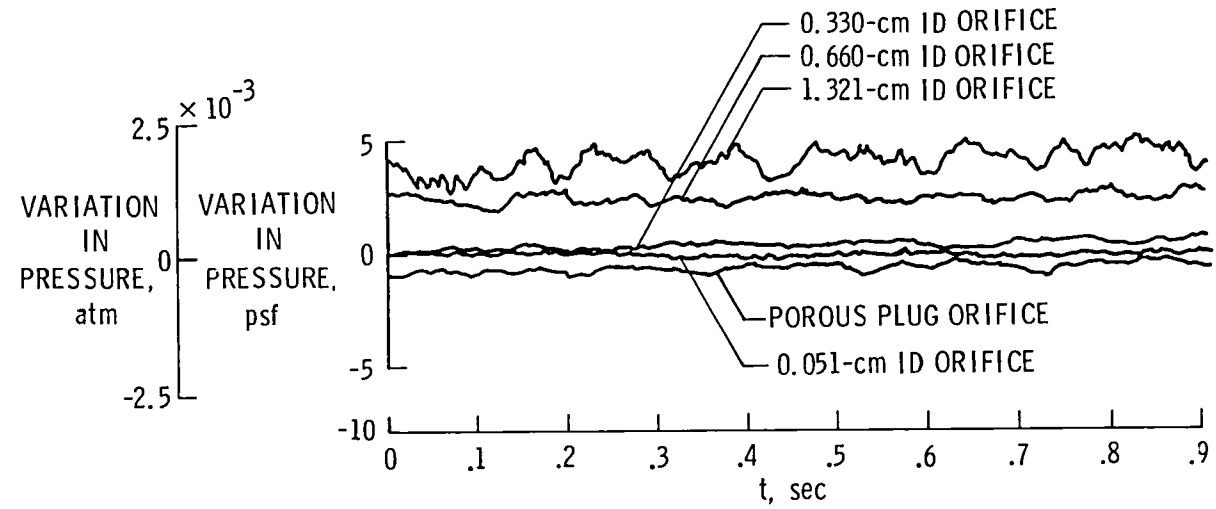

(a) Mach number = 0.40.

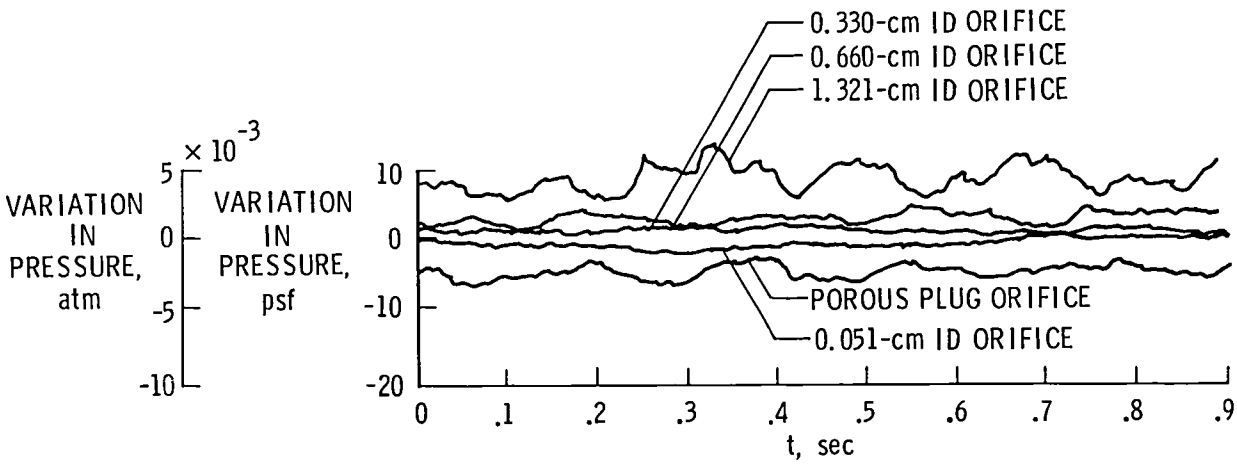

(b) Mach number = 0.72.

Figure 16.- Effect of orifice size on sensed pressure time history.

1. Report No.	2. Government Accession No.	3. Recipient's Catalog No.
NASA TP-2545		

4. Title and Subtitle	5. Report Date
Orifice-Induced Pressure Error Studies in Langley 7- by 10-Foot High-Speed Tunnel	February 1986
	6. Performing Organization Code 505-31-23-07
7. Author(s)	8. Performing Organization Report No.
E. B. Plentovich and Blair B. Gloss	L-16001
	10. Work Unit No.
9. Performing Organization Name and Address	
NASA Langley Research Center Hampton, VA 23665-5225	11. Contract or Grant No.
	13. Type of Report and Period Covered
12. Sponsoring Agency Name and Address	Technical Paper
National Aeronautics and Space Administration Washington, DC 20546-0001	14. Sponsoring Agency Code

15. Supplementary Notes

16. Abstract

For some time it has been known that the presence of a static-pressure measuring hole will disturb the local flow field in such a way that the sensed static pressure will be in error. The results of previous studies aimed at studying the error induced by the pressure orifice were for relatively low Reynolds number flows. Because of the advent of high Reynolds number transonic wind tunnels, a study was undertaken to assess the magnitude of this error at higher Reynolds numbers than previously published and to study a possible method of eliminating this pressure error. This study was conducted in the Langley 7- by 10-Foot High-Speed Tunnel on a flat plate. The model was tested at Mach numbers from 0.40 to 0.72 and at Reynolds numbers from 7.7×10^6 to 11×10^6 per meter (2.3×10^6 to 3.4×10^6 per foot), respectively. The results indicated that as orifice size increased, the pressure error also increased but that a porous metal (sintered metal) plug inserted in an orifice could greatly reduce the pressure error induced by the orifice.

17. Key Words (Suggested by Author(s))	18. Distribution Statement
Pressure measurement Orifices Static pressure Errors Porous materials Flat plates Wind-tunnel tests	Unclassified - Unlimited Subject Category 02

19. Security Classif. (of this report)	20. Security Classif. (of this page)	21. No. of Pages	22. Price
Unclassified	Unclassified	22	A02

For sale by the National Technical Information Service, Springfield, Virginia 22161

NASA-Langley, 1986

National Aeronautics and
Space Administration
Code NIT-4

Washington, D.C.
20546-0001